First round of MaRINET 2 Tidal Energy Round Robin Tests: combined wave and current tests

B. Gaurier, S. Ordonez-Sanchez, J.-V. Facq, G. Germain, C. Johnstone, R. Martinez, I. Santic and F. Salvatore

Abstract—This second Round Robin Test program aims to establish the influence of the combined wave and current effect on the power capture and performance of a generic tidal turbine prototype. In this paper, we present the results obtained in the first two selected facilities: the IFREMER wave and current circulating tank and the CNR-INM wave towing tank. These facilities were selected on the basis that their dimensions along with the rotor diameter of the turbine translate into low blockage ratio conditions and that both facilities can provide the same range of experimental conditions. The experimental campaigns uses the same set-up, except from additional equipment to measure flow characteristics. The performance of the turbine is comparable between the tanks, but because some intrinsic differences in creating wave and current, it may be slightly different for the corresponding conditions. The blockage effect and, in some cases, the velocity disc-integrated averaging need to be accounted for a better agreement. The slight remaining differences observed on the power coefficient curves may be related to turbulence and wave-current interactions. A deeper analysis is required to process the other parameters in order to better understand this phenomena.

Index Terms—Marine energy, wave and current interactions, Round Robin Test, flow measurements, horizontal axis tidal turbine.

I. Introduction

PROTOTYPE testing is an integral part of the development process for many technologies. Testing at small scale can be relatively quick and inexpensive, while testing within a controlled environment enables experiments to be repeated for a range of different parameters. Perhaps one of the main disadvantages associated with experimental research are related to the existence of errors which could potentially lead to an inadequate interpretation of results. These data variations may be related to random or systematic errors which involve the test environment or the appliance. In the case of the performance evaluation of marine energy converters, the test environment may refer to facilities involving flume or tow tanks and the appliance usually refers to the converter and the instrumentation equipment to measure the variables of interest; e.g. power, loads, etc.

A Round Robin Test (RRT) can be designed to enable a first stage quantification of a facility's impact on the technology being tested and on the quality of the tests results. These results are obtained with the same testing program being repeatedly undertaken on the same device model and at a number of test laboratories. As a consequence, better identification and quantification of the investigated causal factors can take place. In addition, such tests can be used to evaluate and improve (if necessary) the specifications given in the international standards: IEC TS 62600-200 to 202 [1]–[3], as explained in [4] or [5].

To establish the influence of the test environment on the power capture and performance of a tidal turbine prototype, a first RRT was undertaken during the FP7 MaRINET project [6]. This programme consisted on testing the exact same $0.7\ m$ diameter horizontal axis tidal turbine in four facilities: two tow and two flume tanks. The turbine was tested at two flow speeds of 0.8 and $1.0\ m/s$. It was found that the average values of power and thrust obtained from the four testing campaigns had small discrepancies. However, the signal fluctuations were higher on the data related to the testing facility that provided the largest blockage ratio (4.8%) and turbulent flows (3%).

A similar analysis was undertaken by [7] where a horizontal axis turbine of $0.8\ m$ was tested at a tow and a flume tank. As an addition to the work developed by [6], the comparative tests involved investigations related to the performance of two types of blade materials: composite and aluminium. The composite blades were specifically designed to enable bend and twist to facilitate load shedding while preserving optimal power output. Similar to the findings presented in [6], it was observed that torque and thrust average values increased slightly when the turbine was operating in the flume facility compared to the data obtained at the tow tank.

Understanding the impact that the extreme marine environment has on the survivability of tidal energy converters is fundamental for the successful development and commercialisation of full scale devices.

B. Gaurier, J.-V. Facq and G. Germain are with the French Research Institute for Exploitation of the Sea (IFREMER), Metocean Laboratory, Boulogne-sur-mer, France (e-mail: bgaurier@ifremer.fr).

S. Ordonez-Sanchez, C. Johnstone and R. Martinez are with the Energy Systems Research Unit (ESRU), Department of Mechanical Engineering, University of Strathclyde, Glasgow, United Kingdom (e-mail: s.ordonez@strath.ac.uk).

I. Santic and F. Salvatore are with the National Research Council, Institute of Marine engineering (CNR-INM), Rome, Italy (e-mail: francesco.salvatore@cnr.it).

Recent efforts from the scientific community to drive the development of tidal technology forward include the estimation of wave loading: *e.g.* [8], [9], [10], [11] and [12] amongst others, or turbulence effects: *e.g.* [13], [14], [15] and [16] amongst others, on tidal energy devices. These investigations cover a wide range of topics ranging from the influences of diverse waveforms, wave directionality, control strategies, turbulent flow characteristics and intensities etc.

Building on these work, a second program is being conducted within the H2020 MaRINET 2 program. The aim of these tests is to replicate the first RRT but extend it by incorporating waves and currents in the testing protocols. An upgraded version of the previous horizontal axis turbine is used for the entirety of the programme. Four laboratories are associated within the working plan and these include the circulating flume tank at IFREMER, the tow tank facility at CNR-INM, the Flowave circulating tank at the University of Edinburgh and the Kelvin hydrodynamics Laboratory tow tank facility at the University of Strathclyde. The first sets of results for the first two rounds of the RRT are presented in this paper.

II. EXPERIMENTAL SET-UP

The first two sets of experiments were carried out at the circulating flume tank available at IFREMER [17] and the tow tank at CNR-INM [18]. These facilities were selected on the basis that their dimensions along with the rotor diameter of the turbine translate into low blockage ratio conditions, as seen in table I. The turbine axis was kept at a constant depth of $1.0\ m$ in each facility and a variety of instruments to measure the flow conditions were mounted in close proximity to the turbine. Further details of the flow monitoring are presented in Section II-C.

Fig. 1. The 3-bladed instrumented turbine in the wave and current flume tank of IFREMER (top) and in the towing tank of CNR-INM (bottom)

TABLE I
TESTING FACILITIES MAIN CHARACTERISTICS

Laboratory name	IFREMER	CNR-INM
Type of tank	flume	towing
Length [m]	18	220
Width × depth [m^2]	4 × 2	9 × 3.5
Speed range [m/s]	0.1 to 2.2	0.1 to 10
Turbulence int. [%]	1.5 to 15	NA
Blockage ratio [%]	5.1	1.3

The turbine (shown in Figure 1) was fixed on a moving carriage in the towing tank and on a customised mounting frame in the flume tank.

A. Turbine prototype specifications

A three bladed horizontal axis turbine developed by IFREMER is used in this RRT campaign. The turbine is $0.724\ m$ in diameter (D) and a motor speed control unit is used to set various turbine rotational speeds. The blades are exactly the same as in [6] which were designed based on a NACA 63-418 profile.

The advanced prototype is equipped with a dedicated load cell in each blade root, following the designed proposed by [19]. The load cell is capable to measure 5 different channels: 2 forces and 3 moments.
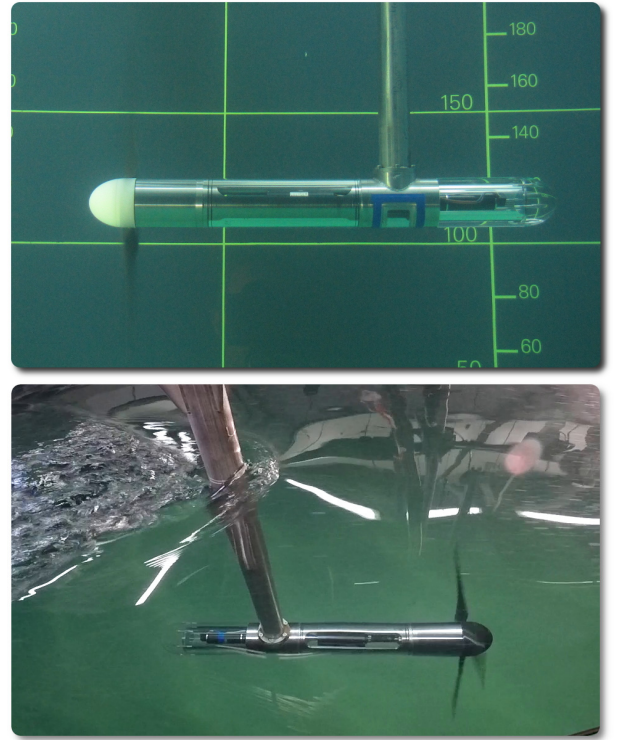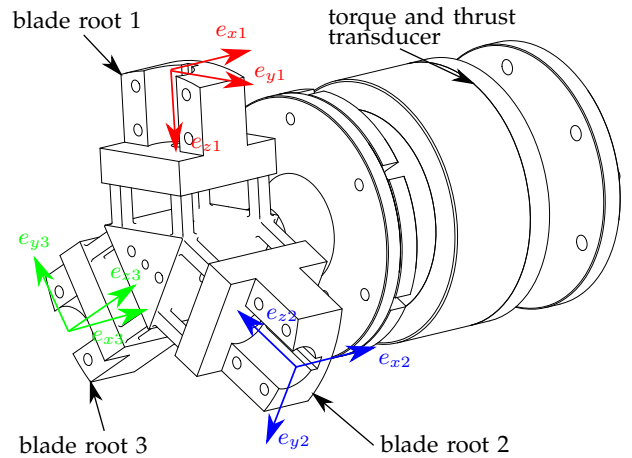

Fig. 2. The blade root load-cell with its three coordinate systems and the torque and thrust transducer. All these sensors are waterproof.

E.g., for blade B1 (figures 2 and 3), the measured forces are the ones along e_{x1} (blade contribution to thrust) and e_{y1} (blade contribution to torque), and the three moments around e_{x1} (edgewise bending moment), e_{y1} (flapwise bending moment) and e_{z1} (pitching moment). The same measurements are done on blades B2 and B3 with the same components: [F_{xi}; F_{yi}; M_{xi}; M_{yi}; M_{zi}] with $i = 1$ to 3 in the corresponding blade coordinate system. For every blade coordinate system, e_{xi} is the streamwise direction, e_{yi} is opposed to the rotation direction and e_{zi} is oriented towards the centre of rotation (figures 2 and 3).

In addition to this multi-component load-cells, the torque and thrust applied on the main rotation axis of the rotor are measured as well. This waterproof
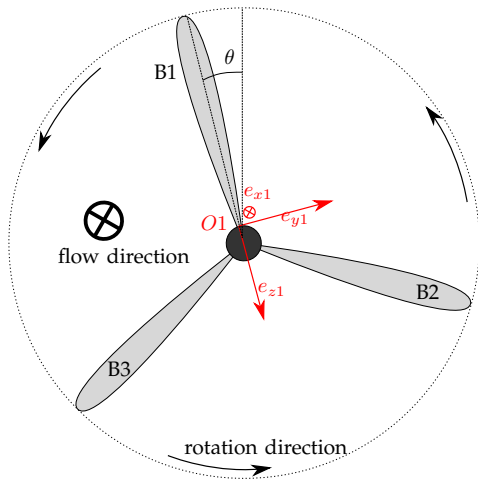
Fig. 3. Schematic of the turbine facing the flow, with the blade B1 root coordinate system. θ stands for the turbine angle of rotation, with $\theta = 0$ corresponding to the time when blade B1 is vertical at the top.

transducer is positioned upstream of the seals of the machine to prevent measuring friction effects (figure 2). The blade root load-cell and the torque and thrust transducer are custom made by the French company Sixaxes [20] in partnership with IFREMER. The shielded cables coming from these transducers are routed through a slip-ring enabling the free rotation of the cables while prevent their entanglement. These low voltage signals are amplified by an electronic signal processing unit, located outside of the turbine and on the dry. The signal amplification is not possible inside the turbine because of the restricted volume. However, the shielded cables and the the slip-ring quality limit the noise in the low-voltage analogue signals. The motor shaft is connected to the turbine shaft through a motor-gearbox facilitating the acquisition of suitable torque and rotation speed ratings.

All signals are acquired using National Instruments hardware and in-house electronics developed by IFREMER staff. The signals are sampled at a frequency (f_s) of $120\ Hz$. Flow measurements and water surface elevation are also utilised and synchronised with the turbine instrumentations by means of a short impulse trigger signal.

B. Experimental plan

The first part of the testing campaign including the turbine, comprises tests without wave interactions, thus the flow velocity or carriage velocity is set to 0.8 and 1.0 m/s until a full power curve has been established with at least ten points to construct the performance curves corresponding to the turbine. These curves are based on the non dimensional parameters: $C_P - TSR$ curves which are defined below:

$$C_P = \frac{Q\omega}{0.5\rho A U_\infty^3} \tag{1}$$

$$TSR = \frac{\omega R}{U_\infty} \tag{2}$$

where Q is the mean hydrodynamic torque (in $N.m$) generated by turbine, obtained from the transducer. The angular velocity of the turbine is represented by ω in rad/s. The turbine radius (R) is $0.362\ m$ and A stands for the rotor swept area (πR^2). The density of the water was considered in these calculations as $1000\ kg/m^3$. Power coefficient (C_P) is presented in relation to the Tip Speed Ratio (TSR). This non-dimensional value defines the ratio between the blade tip speed ($\omega \times R$) and the tow/flow velocity (U_∞), as shown in equation 2. The flow velocity was estimated using the measurements from two instruments when possible, as explained in Section II-C.

The second part of the testing includes four regular waves in-line with the current, as observed in table II. For each of the test cases eleven TSR were considered ranging from 0 to 7. To quantify the uncertainty of the experiment, repeated tests were considered for each case for several TSR. Due to limitations with the equipment at CNR-INM, the test matrix was constricted to only five TSR per case and two TRS for the repeated tests.

TABLE II
SUMMARY OF THE TEST MATRIX

Case	Type	Flow speed [m/s]	Wave freq. [Hz]	Wave height [mm]
1	current	0.8		
2	regular	0.8	0.6	150
3	regular	0.8	0.5	70
4	current	1.0		
5	regular	1.0	0.7	150
6	regular	1.0	0.6	110

C. Flow measurement and characterisation

The flow stream was characterised while the turbine was in operation using an Acoustic Doppler Velocimeter (ADV). This was placed in line with the turbine hub at a distance of $1.2\ m$ along the cross section of the tank (see figure 4). At IFREMER, seeding particles were deposited in the tank and continuous flow circulation permitted a uniform dispersion in the flow stream. For the experiments at CNR-INM, a seeding mast was placed $4.0\ m$ upfront of the ADV.

In addition to the ADV, the flow was also monitored using a Laser Doppler Velocimeter (LDV) during the first testing campaign at IFREMER. While the ADV is able to measure three flow velocity components, the LDV available at IFREMER can capture two components: u which is related to the flow direction e_x and v the horizontal component related to e_y. The LDV was installed 2 diameters (D) upstream from the turbine. The focal point of the laser beam was set to be inline with the turbine hub, at $1.0\ m$ water depth.

A number of wave probes were also placed next to the turbine to verify the wave parameters set for each of the case scenarios. Three resistive wave probes were used at the facility in IFREMER: probes 1-3 as seen in figure 4. A mix of resistive, ultrasound and dynamic wave probes were used in the CNR-INM tow tank: probes 3-6 as seen in figure 4, where probes 4
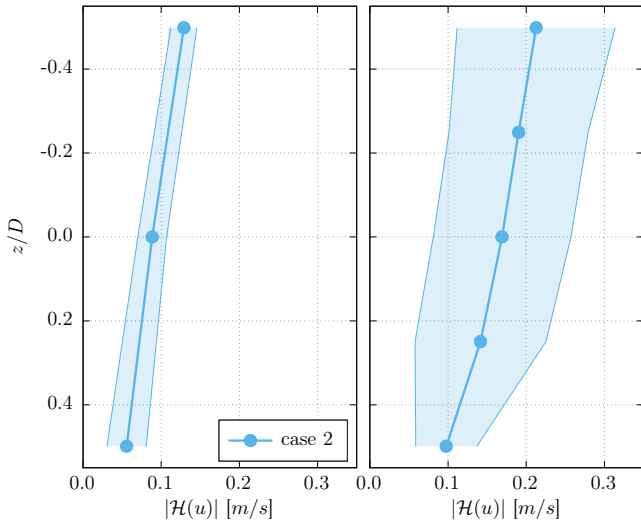
Fig. 4. Schematic top-view of the test set-up used in the two tanks. ADV was used at IFREMER and CNR-INM. LDV was only used at IFREMER and carriage speed is only measured at CNR-INM. The seeding mast was required at CNR-INM only. The wave gauges 1 to 3 were used at IFREMER and 3 to 6 at CNR-INM.

and 6 were ultrasound wave gauges and probe 5 was a dynamic wave gauge. One single identical resistive wave probe was used in all facilities (probe 3). This is a crucial aspect of the test campaign, especially since the flow characteristics affected by the addition of waves is deemed to be relevant between facilities.

III. INFLOW VELOCITY ANALYSIS

Velocity measurement profiles have been performed in each of the testing facilities recording the flow variations without the turbine. These profiles are shown on figure 5 with three points for CNR-INM at the left hand-side and fives points for IFREMER at the right-hand side, covering the turbine diameter height; $z/D = 0$ stands for the depth of the turbine rotation axis. The averaged velocity is slightly different between the tanks for case 1: 0.848 m/s for CNR-INM and 0.813 m/s for IFREMER.

Additional points are required at IFREMER flume tank especially because the wavemaker is intrusive and located upstream of the turbine area. This mainly explains the reason why the profile is non-linear for case 2, with a difference of more than 0.2 m/s in the averaged velocity between the top and bottom points. The turbulent intensity increases as well because of the wavemaker presence explaining the larger standard-deviation for the same case. Moreover, in this tank, waves are superimposed to the flow which generates a real interaction between waves and current. Finally, for all the wave and current cases performed at IFREMER flume tank, a velocity average covering the entire turbine disc is necessary in order to account for these phenomena. On the contrary, in the tow tank, the vertical profiles are identical. Only the standard-deviation increases for case 2 because of the orbital velocities created by the waves.

The orbital velocities are quantified on figure 6 showing the time averaged and standard-deviation of the

Fig. 5. Vertical profile of the time averaged and standard-deviation of the ADV streamwise velocity, versus the depth (z/D) for cases 1 and 2 at the CNR-INM towing tank (left) and IFREMER flume tank (right)

amplitude of the Hilbert transform of the u component of the ADV velocity signal $|\mathcal{H}(u)|$, for case 2 and the same points z/D. The large standard-deviation observed for the IFREMER flume tank indicates a variation of the amplitude of the waves created in this tank. This is mainly caused by the wavemaker presence and the turbulence intensity. It is not the same for CNR-INM tow tank where the standard-deviation stays always low. In addition, a slight difference ($\leq 0.1m/s$) in term of averaged velocity amplitude is noticeable between the tanks, for all the points.

During an acquisition, the ADV measures the flow velocity in synchronisation with the turbine parameters at $z/D = 0$. Looking at the variation of this
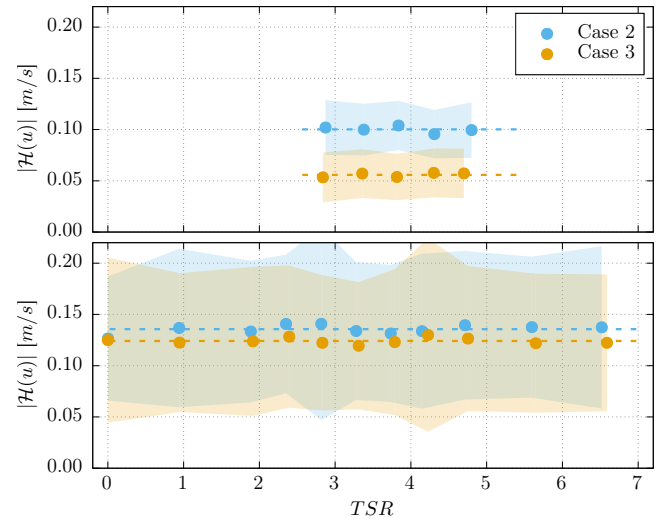
Fig. 6. Time average and standard-deviation of the amplitude of the Hilbert transform of the ADV streamwise velocity versus the depth (z/D) for case 2 at the CNR-INM towing tank (left) and IFREMER flume tank (right)

recorded flow velocity leads to figure 7 for cases 2 and 3, versus the turbine TSR. Whereas the average velocity is very close at CNR-INM, a slight difference is noticeable between cases at IFREMER. The wave and current interactions in the flume tank can explain such a difference. As already observed, the standard-deviation which mainly comes from the wave orbital velocity and turbulence, is higher for the flume tank.
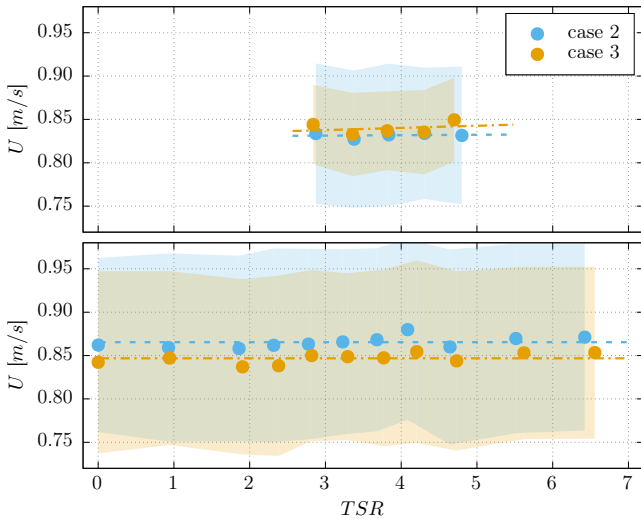
Fig. 7. Time average and standard-deviation of the ADV streamwise velocity versus turbine TSR for cases 2 and 3 at CNR-INM towing tank (top) and IFREMER flume tank (bottom)

Following the same procedure, figures 8 and 9 show the amplitude of the Hilbert transform of the free surface elevation η and of the streamwise velocity u respectively, versus the TSR.

The averaged free surface elevations are very close between the tanks: $[66; 30]$ mm for CNR-INM and $[73; 34]$ mm for IFREMER, for cases 2 and 3 respectively (figure 8). However, the standard-deviation is really different: small values for CNR-INM, but large ones for IFREMER. This indicates the waves are very similar in

the tow tank, but their amplitude vary largely in the flume tank.
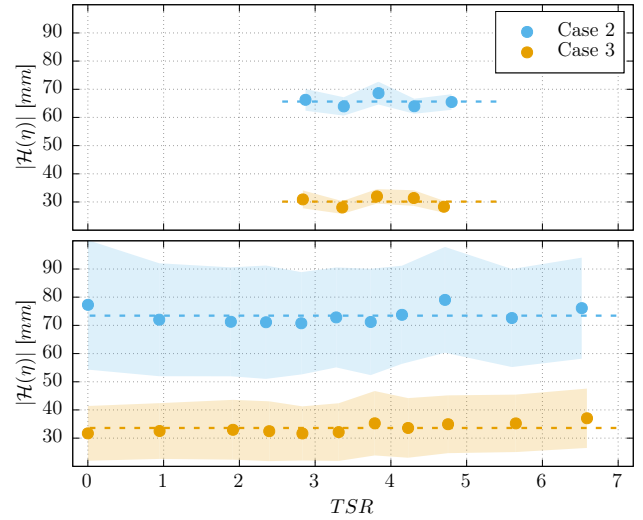
Fig. 8. Time average and standard-deviation of the amplitude of the Hilbert transform of the free surface elevation η measured by wave gauge 3 versus the TSR for cases 2 and 3 at CNR-INM towing tank (top) and IFREMER flume tank (bottom)

Fig. 9. Time average and standard-deviation of the amplitude of the Hilbert transform of the streamwise velocity versus the TSR for cases 2 and 3 at CNR-INM towing tank (top) and IFREMER flume tank (bottom)

As previously observed in figure 6 for case 2, the averaged orbital velocities are larger for the IFREMER flume tank: $[0.100; 0.056]$ m/s for CNR-INM and $[0.136; 0.124]$ m/s for IFREMER, for cases 2 and 3 respectively (figure 9). These larger values measured in the flume tank can be surprising, especially for case 3. Indeed, the surface elevation is rather close between tanks (figure 8). However, the wave and current interaction and the turbulence can explain such a difference.

Finally, all these differences are mainly related to the intrinsic characteristics of the tanks and may be a source of uncertainty when comparing the performance results of a marine turbine.

IV. PERFORMANCE COMPARISONS

In this section, we study the performance results of the marine turbine model described in II-A obtained in both tow and flume tanks.

D. Power coefficient comparison without wave

Considering the flow velocity measured by the ADV in synchronisation with the turbine parameters in formula 1 and 2, we obtain the figure 10 for the C_P versus TSR curves and for current only cases (1 and 4), for both tanks.
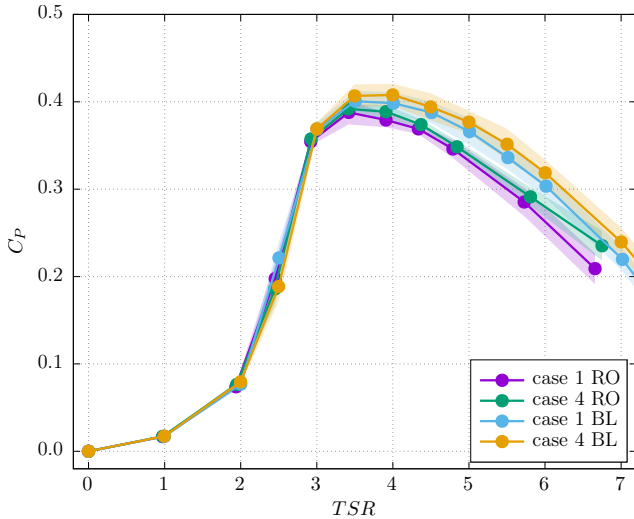

Fig. 10. Power coefficient C_P for cases 1 and 4 (current only) versus TSR, for CNR-INM (RO) and IFREMER (BL) tanks

First of all, these results look pretty similar. They are identical for $TSR \leq 3$ but start to spread out from that point. Despite that the difference between curves stays very low, two different groups appear from $TSR \geq 4$: the first group with the largest values for the IFREMER flume tank and the second group with the lower values for CNR-INM. Inside each group, C_P are slightly larger for case 4 comparing to case 1. This last remark can be explain by the Reynolds effect, as already observed in [6]. In addition, the difference noticed between the groups, *i.e.* between the tanks, can be mainly explained by the blockage ratio. Indeed, as seen in table I, although the blockage ratio is small, it is 5 times higher at IFREMER comparing to CNR-INM. In the previous paper [6], authors used the method coming from [21] to compensate the difference in term of blockage effect. Applying the same method on these results leads to the blockage correction factor $(U_T/U_F)^3$ depicted on figure 11 for the power coefficient.

These correction factors are slightly different from the ones presented in [6]. They are based on the relative size of the facility and on the measured thrust coefficient. During the previous RRT, the thrust was not measured on the turbine rotor, but from a load-cell based on the top part of the supporting mast. In order to remove the drag part from the mast, authors subtracted the drag measured at $TSR = 0$ to the one measured at every other TSR. That leads
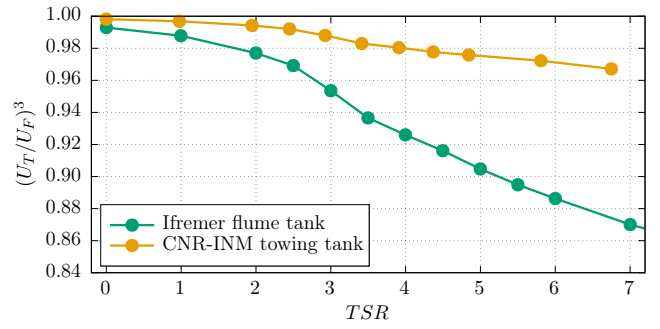

Fig. 11. Blockage correction factor $(U_T/U_F)^3$ versus TSR to be applied to the power coefficient according to the method presented in [21]

to slight difference for the CNR-INM tank but larger difference for the IFREMER flume tank: for $TSR = 7$, $(U_T/U_F)^3 = 0.87$ when it was 0.93 in [6].

Applying these blockage correction factors to the power coefficients previously shown leads to the figure 12. The blockage corrections clearly improve the curves decreasing the differences between the tanks for $TSR \geq 4$.
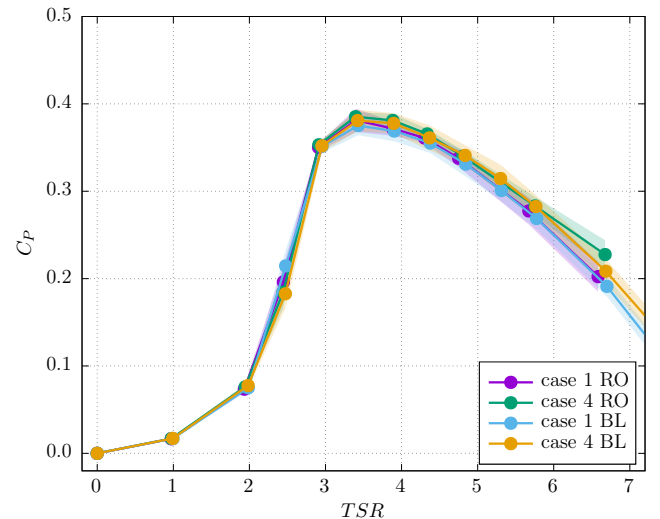

Fig. 12. Power coefficient C_P for cases 1 and 4 (current only) versus TSR, for CNR-INM (RO) and IFREMER (BL) tanks, accounting for the blockage correction factor

E. Power coefficient comparison with wave

As seen in section III, the velocity profile in the IFREMER flume tank shows a vertical gradient when the wavemaker is used. In order to account for this gradient perceived by the turbine, a disc-integrated average is performed from the velocity measurements carried out without the turbine. This corresponds to the method described in [22]. In addition, for all the cases with such a vertical gradient, a particular attention is paid to the processing of the power coefficient: the cubing of the velocity has to be performed prior to temporal and spatial averaging, as shown by [23].

As a consequence, the ADV measurement point carried out in synchronisation with the turbine parameters is used as the centre point of a disc with a diameter D

and showing a vertical gradient profile corresponding to the one measured previously without the turbine, as seen in figure 5 for case 2. Then, the disc-integrated average is performed. And finally, an equivalent velocity is used in formula 1 and 2, based on coefficients C^n:

$$C^n = \frac{\overline{\overline{u^n}^t}^d}{\overline{\overline{u^n}^t}^p} \qquad (3)$$

where $\overline{u}^t$ stands for the time averaging and $\overline{u}^p$ or $\overline{u}^d$ stand for centre point or the spatial disc-integrated averaging respectively. Note that the velocity is powered (n) prior to temporal and spatial averaging. C^1 is used for the velocity expressed in the TSR formula, whereas C^3 is required for the one corresponding to the C_P formula (the C_T formula needs C^2). Coefficients C^n are given in table III for all the wave and current cases.

TABLE III
COEFFICIENTS C^n USED FOR THE TSR, C_T AND C_P PROCESSING IN ORDER ACCOUNT FOR THE VERTICAL VELOCITY GRADIENT FOR WAVE AND CURRENT CASES AT IFREMER. THESE COEFFICIENTS ARE BASED ON THE VELOCITY PROFILES MEASURED WITHOUT THE TURBINE.

Case	C^1	C^2	C^3
2	0.985	0.975	0.968
3	0.995	0.995	0.997
5	0.990	0.983	0.979
6	0.981	0.968	0.958

The results obtained with this processing method, only applied for the IFREMER flume tank data, are shown on figures 13 and 14 and compared to the C_P from the CNR-INM tow tank. The blockage correction factor, explained in the previous section IV-D is applied as well.
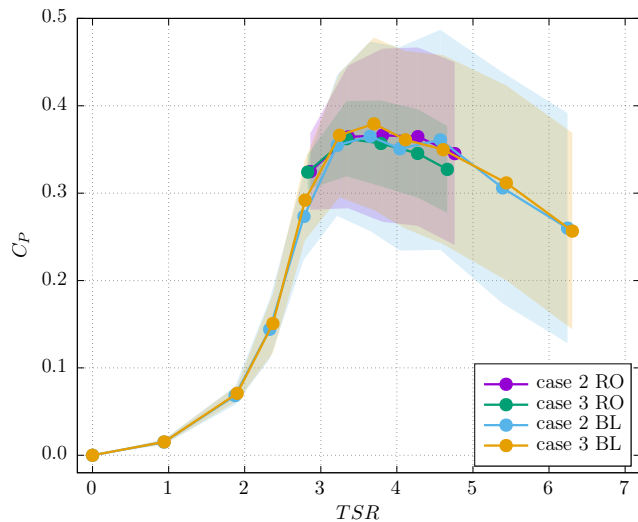

Fig. 13. Power coefficient for cases 2 and 3 versus TSR, for CNR-INM (RO) and IFREMER (BL) tanks, accounting for the blockage correction factor and the velocity disc-integrated averaging

These curves are in relatively good agreement, especially for cases 2 and 3. Indeed, on figure 13, only the curve obtained for case 3 in the CNR-INM tow tank is slightly lower from the others. In addition, it is clearly noticeable that the corresponding standard-deviation is lower from the others as well.
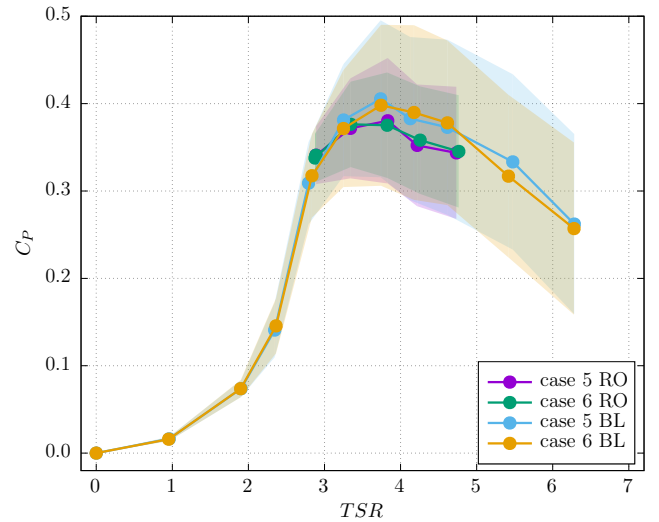

Fig. 14. Power coefficient for cases 5 and 6 versus TSR, for CNR-INM (RO) and IFREMER (BL) tanks, accounting for the blockage correction factor and the velocity disc-integrated averaging

On figure 14, the difference is larger between tanks. The average of the C_P is lower for the CNR-INM from $TSR \geq 4$. In addition, the standard-deviation is lower as well, for the same range of TSR, comparing to the same results at IFREMER. As noticed in section III the standard-deviation of the inflow velocity, the surface elevation and the orbital velocity are higher is the flume tank. This could explain the higher standard-deviation of the power coefficient observed on this curve.

In order to better understand the difference on the power coefficient curves, we propose now to focus on a particular point: $TSR = 4$ for case 6.

F. A particular wave and current test comparison

In the following part, a deeper analysis is given on a particular test acquisition. Figures 15 and 17 show the input parameters recorded in IFREMER and CNR-INM respectively. These parameters are the surface elevation η from wave gauge 3 and the streamwise velocity u measured by the ADV. As shown on these figures, η and u show larger amplitudes at the IFREMER flume tank. On the contrary, amplitudes are lower but more regular with time at the towing tank. This corresponds to what has already been observed in section III.

In the same way, the turbine parameters represented by the rotation speed ω, the torque Q and the power P are depicted on figures 16 and 18 for the same period of time and for IFREMER and CNR-INM tanks respectively. As observed for the input characteristics, the turbine parameters are more periodic at the towing tank, but show higher amplitude of variation at the flume tank.

The table IV summarizes the time average and standard-deviation values for the parameters displayed on figures 15 to 18. It is clear that the averaged values obtained for the rotation speed ω are very close between the tanks. Concerning the averaged
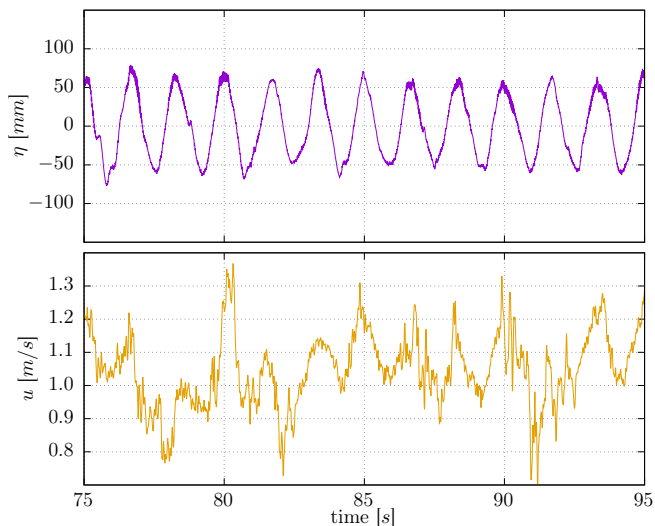
Fig. 15. Extract of the time history of the input parameters (wave amplitude η and velocity u) recorded at IFREMER flume tank for case 6 and $TSR = 4$
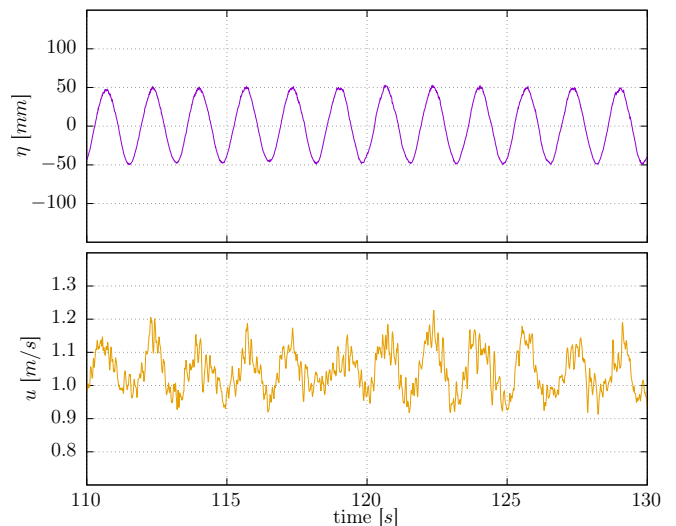

Fig. 17. Extract of the time history of the input parameters (wave amplitude η and velocity u) recorded at CNR-INM towing tank for case 6 and $TSR = 4$
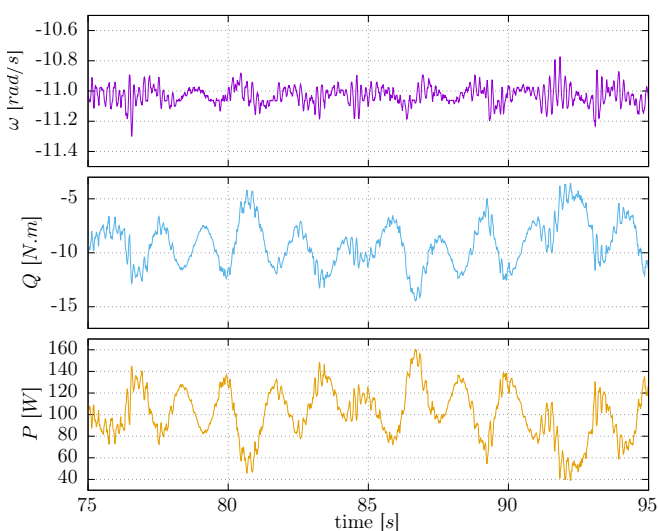

Fig. 16. Extract of the time history of the turbine parameters (rotation speed ω, torque Q and power P) recorded at IFREMER flume tank for case 6 and $TSR = 4$
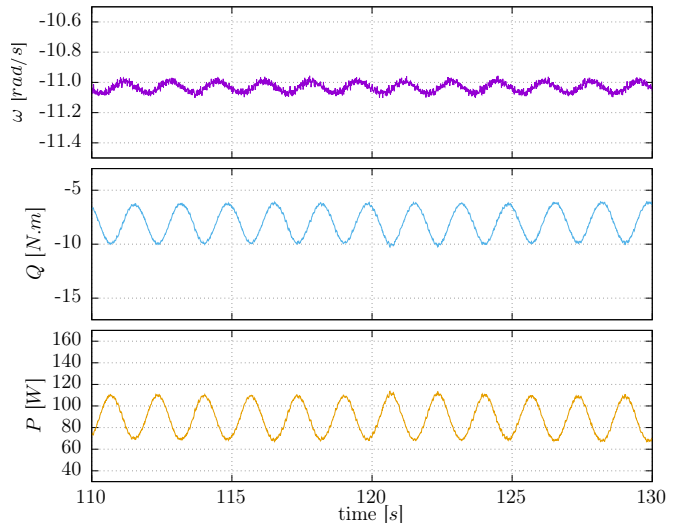

Fig. 18. Extract of the time history of the turbine parameters (rotation speed ω, torque Q and power P) recorded at CNR-INM towing tank for case 6 and $TSR = 4$

velocity u, the difference of about $0.02\ m/s$ (equivalent to 2%) disappears when considering the disc-integrated averaging (for the IFREMER value, cf. table III): $1.061 \times 0.981 = 1.041\ m/s$ which is very close to the value measured at CNR-INM ($1.037\ m/s$). However, the mean of the torque Q is higher by more than $1\ N.m$ (in absolute value) at IFREMER. With a rotation speed of about $11\ rad/s$, this difference leads to about $15\ W$ difference in the final power value. Accounting for the blockage coefficients presented on figure 11, a difference of $8\ W$ is still persistent, explaining the difference observed on figure 14 for the C_P.

However, this difference of about $1\ N.m$ noticed on the averaged torque is lower than the corresponding standard-deviation value. Except for the rotation speed, the other standard-deviation values are about twice as high for IFREMER flume tank than for CNR-INM. As explained before, the turbulence intensity is higher for IFREMER flume tank and this turbulence

TABLE IV
TIME AVERAGE AND STANDARD-DEVIATION OF SOME OF THE PARAMETERS MEASURED FOR CASE 6 AND $TSR = 4$, CORRESPONDING TO FIGURES 15 TO 18

Parameter	IFREMER		CNR-INM	
	$\overline{x}$	$\sigma(x)$	$\overline{x}$	$\sigma(x)$
$u\ [m/s]$	1.061	0.120	1.037	0.065
$\omega\ [rad/s]$	-11.029	0.054	-11.032	0.030
$Q\ [N.m]$	-9.456	2.178	-8.101	1.296
$P\ [W]$	104.320	24.141	89.444	14.353

increase may explain this torque difference. Indeed, comparing figures 13 and 14, when the C_P standard-deviation is equivalent, *e.g.* for case 2, the C_P average is similar. However, when the C_P standard-deviation is lower for CNR-INM, the C_P average is lower as well (cases 3, 5 and 6). In addition, as seen previously, the C_P standard-deviation mainly comes from the torque standard-deviation, which is strongly linked with the low frequency components of the input velocity, according to [15]. For these tests, the low

frequency components of the velocity mainly come from the orbital velocity of the wave, the wave-current interaction and turbulence. So, as a first attempt, the turbulence and wave-current interaction at IFREMER flume tank seem to be responsible for the increase of the averaged torque.

A deeper analysis of the blade forces and moments depending on the phase between their respective positions and the surface waves will enable to better understand this phenomena.

V. CONCLUSION AND PERSPECTIVES

This paper presents the first results obtained into the first two facilities of the tidal MaRINET 2 Round Robin Test. Four laboratories are associated within the working plan, but only the flume tank at IFREMER and the tow tank at CNR-INM have already been used yet. This new Round Robin Test replicates the previous program, *i.e.* keeping constant the turbine model and testing instruments, but extend it by incorporating waves and currents in the testing protocols.

As observed in the inflow velocity analysis, the hydrodynamic conditions are close between both facilities. However, several slight differences appear, especially in terms of standard-deviation, mainly due to turbulence and wave-current interaction obtained at IFREMER flume tank. These differences are related to the intrinsic characteristics of the tanks.

The power coefficients versus Tip Speed Ratio are presented for current and wave-current cases and for both facilities. These first results are in good agreement but need to be corrected, considering the blockage effect and the disc-integrated averaging when the velocity profile shows a vertical gradient, as in IFREMER flume tank with the wavemaker.

Finally, a particular case analysis shows that when a difference is noticed on the averaged power coefficient, this seems to be only related to a torque difference. This gap in the measured torque between facilities may be linked with the difference observed in the inflow velocity analysis: *i.e.* the turbulence and wave-current interactions.

A deeper analysis is however require to further explore the variations of the blade forces and moments obtained for each wave condition at both facilities. This should enable to better understand this phenomena. In addition, the next tests are planned at Flowave (University of Edinburgh) and Kelvin Hydrodynamic Laboratory (University of Strathclyde) before the end of the year. They will bring new wave-current flow conditions and certainly new interesting results.

ACKNOWLEDGMENT

REFERENCES

[1] Marine Energy, "Wave, tidal and other water current converters - Part 200: Electricity producing tidal energy converters - Power performance assessment," International Electrotechnical Commission, Tech. Rep. 27.140, 2013. [Online]. Available: https://webstore.iec.ch/publication/7242

[2] ——, "Wave, tidal and other water current converters - Part 201: Tidal energy resource assessment and characterization," International Electrotechnical Commission, Tech. Rep. 27.140, 2015. [Online]. Available: https://webstore.iec.ch/publication/22099

[3] ——, "Wave, tidal and other water current converters - Part 202: Scale testing of tidal stream energy systems," International Electrotechnical Commission, Tech. Rep., 2019.

[4] G. Germain, A. Chapeleau, B. Gaurier, L.-M. Macadre, and P. Scheijground, "Testing of marine energy technologies against international standards. Where do we stand?" in *Proceedings of the 12th European Wave and Tidal Energy Conference*, Cork, Ireland, 2017. [Online]. Available: http://www.ewtec.org/proceedings/

[5] G. Germain, B. Gaurier, M. Harrold, M. Ikhennicheu, P. Scheijgrond, A. Southall, and M. Träsch, "Protocols for testing marine current energy converters in controlled conditions. Where are we in 2018?" in *Proceedings of the 4th Asian Wave and Tidal Energy Conference*, Taipei, Taiwan, 2018. [Online]. Available: http://www.awtec.asia/proceedings/

[6] B. Gaurier, G. Germain, J.-V. Facq, C. Johnstone, A. Grant, A. Day, E. Nixon, F. Di Felice, and M. Costanzo, "Tidal energy "Round Robin" tests comparisons between towing tank and circulating tank results," *International Journal of Marine Energy*, vol. 12, pp. 87 – 109, 2015, special Issue on Marine Renewables Infrastructure Network. [Online]. Available: http://www.sciencedirect.com/science/article/pii/S2214166915000223

[7] R. E. Murray, S. Ordonez-Sanchez, K. E. Porter, D. A. Doman, M. J. Pegg, and C. M. Johnstone, "Towing tank and flume testing of passively adaptive composite tidal turbine blades," in *Proceedings of the 12th European Wave and Tidal Energy Conference*, Cork, Ireland, 2017. [Online]. Available: http://www.ewtec.org/proceedings/

[8] B. Gaurier, P. Davies, A. Deuff, and G. Germain, "Flume tank characterization of marine current turbine blade behaviour under current and wave loading," *Renewable Energy*, vol. 59, pp. 1 – 12, 2013. [Online]. Available: http://www.sciencedirect.com/science/article/pii/S0960148113001353

[9] P. W. Galloway, L. E. Myers, and A. S. Bahaj, "Quantifying wave and yaw effects on a scale tidal stream turbine," *Renewable Energy*, vol. 63, pp. 297 – 307, 2014. [Online]. Available: http://www.sciencedirect.com/science/article/pii/S09960148113004977

[10] R. Martinez, G. S. Payne, and T. Bruce, "The effects of oblique waves and currents on the loadings and performance of tidal turbines," *Ocean Engineering*, vol. 164, pp. 55 – 64, 2018. [Online]. Available: http://www.sciencedirect.com/science/article/pii/S0029801818309296

[11] S. Ordonez-Sanchez, M. Allmark, K. Porter, R. Ellis, C. Lloyd, I. Santic, T. O'Doherty, and C. Johnstone, "Analysis of a horizontal-axis tidal turbine performance in the presence of regular and irregular waves using two control strategies," *Energies*, vol. 12, no. 3, 2019. [Online]. Available: http://www.mdpi.com/1996-1073/12/3/367

[12] S. Draycott, G. Payne, J. Steynor, A. Nambiar, B. Sellar, and V. Venugopal, "An experimental investigation into non-linear wave loading on horizontal axis tidal turbines," *Journal of Fluids and Structures*, vol. 84, pp. 199 – 217, 2019. [Online]. Available: http://www.sciencedirect.com/science/article/pii/S0889974618305073

[13] J. McNaughton, S. Harper, R. Sinclair, and B. Sellar, "Measuring and modelling the power curve of a commercial-scale tidal turbine," in *Proceedings of the 11th European Wave and Tidal Energy Conference*, Nantes, France, 2015. [Online]. Available: http://www.ewtec.org/proceedings/

[14] O. Durán Medina, F. G. Schmitt, R. Calif, G. Germain, and B. Gaurier, "Turbulence analysis and multiscale correlations between synchronized flow velocity and marine turbine power production," *Renewable Energy*, vol. 112, pp. 314 – 327, 2017. [Online]. Available: http://www.sciencedirect.com/science/article/pii/S0960148117304093

[15] B. Gaurier, G. Germain, and G. Pinon, "How to correctly measure turbulent upstream flow for marine current turbine performance evaluation?" in *Proceedings of the 3rd International Conference on Renewable Energies Offshore*, Lisbon, Portugal,

2018. [Online]. Available: http://www.centec.tecnico.ulisboa.pt/renew2018/

[16] B. Gaurier, M. Ikhennicheu, G. Germain, and J.-V. Facq, "Experimental effect of the wake of a wide wall-mounted obstacle on a marine current turbine," in *Proceedings of the 16èmes Journées de l'Hydrodynamique*, Marseille, France, 2018. [Online]. Available: https://jh2018.sciencesconf.org/

[17] B. Gaurier, G. Germain, J.-V. Facq, and T. Bacchetti, "Wave and current flume tank of Boulogne-sur-mer. Description of the facility and its equipment." IFREMER, Tech. Rep. 19CSMBL18, 2018. [Online]. Available: https://archimer.ifremer.fr/doc/00470/58163/

[18] Consiglio Nazionale delle Ricerche. (2018) Towing tanks. [Online]. Available: http://www.insean.cnr.it/en/content/towing-tanks

[19] G. S. Payne, T. Stallard, and R. Martinez, "Design and manufacture of a bed supported tidal turbine model for blade and shaft load measurement in turbulent flow and waves," *Renewable Energy*, vol. 107, pp. 312 – 326, 2017. [Online]. Available: http://www.sciencedirect.com/science/article/pii/S0960148117300782

[20] Sixaxes. (2017) Société française, spécialisée dans l'étude et la fabrication de chaîne de mesure de force depuis plus de 22 ans. [Online]. Available: http://www.sixaxes.com/

[21] A. Bahaj, A. Molland, J. Chaplin, and W. Batten, "Power and thrust measurements of marine current turbines under various hydrodynamic flow conditions in a cavitation tunnel and a towing tank," *Renewable Energy*, vol. 32, no. 3, pp. 407 – 426, 2007. [Online]. Available: http://www.sciencedirect.com/science/article/pii/S0960148106000516

[22] P. Mycek, B. Gaurier, G. Germain, G. Pinon, and E. Rivoalen, "Experimental study of the turbulence intensity effects on marine current turbines behaviour. Part I: One single turbine," *Renewable Energy*, vol. 66, pp. 729 – 746, 2014. [Online]. Available: http://www.sciencedirect.com/science/article/pii/S096014811400007X

[23] T. Blackmore, L. E. Myers, and A. S. Bahaj, "Effects of turbulence on tidal turbines: Implications to performance, blade loads, and condition monitoring," *International Journal of Marine Energy*, vol. 14, pp. 1 – 26, 2016. [Online]. Available: http://www.sciencedirect.com/science/article/pii/S2214166916300297